Dispersive and nondispersive phase shifts in atomic Stern-Gerlach interferometry

O. Gorceix, J. Robert, S. Nic Chormaic,* Ch. Miniatura, and J. Baudon
Laboratoire de Physique des Lasers, Université Paris–Nord, Avenue J. B. Clément, 93430 Villetaneuse, France
(Received 15 March 1994)

We present experimental results on metastable hydrogen-beam Stern-Gerlach interferometry using either static magnetic fields or time-dependent magnetic fields. The shared experimental scheme is presented. The dispersive behavior of the induced phase shift in the static situation is evidenced. The time-dependent (pulsed) scheme has provided experimental evidence for an external wave-function phase shift in atom force-free dynamical evolution. This so-called scalar Bohm-Aharonov (SAB) effect is thoroughly investigated. As opposed to the static field case, the nondispersive behavior of the SAB effect is validated. Experiments that mix static and pulsed magnetic fields are performed to reach the provisional goal to test nontrivial phase additivity. In all cases, experimental results are shown to be consistent with theoretical predictions derived from a tentative model including the deterministic magnetic phase shifts as well as additional random shifts due to experimental imperfections.

PACS number(s): 03.75.Dg, 03.65.Bz

I. INTRODUCTION

Atom interferometry has attracted increased research interest in recent years with the realization of several practical devices. Such interferometers have already been used for studies of interaction effects acting on atomic motion as well as for fundamental tests of quantum theory [1]. In previous papers [2,3], we showed that a device based on the longitudinal Stern-Gerlach effect gives opportunities for atom phase investigations. There, static magnetic-field gradients were being used both for the realization of the interferometer elements and for the phase object. The present paper is aimed at providing experimental evidence that time-dependent magnetic fields can be used as well. As shown in an earlier paper [4], substantially different results are obtained with pulsed fields as compared to static fields. The present paper is an extension of this work; it involves a detailed validation of the scalar Bohm-Aharonov (SAB) effect in atomic interferometry.

The paper is organized as follows. In Sec. II, the basic Stern-Gerlach interferometry (SGI) experimental method is described. In Sec. III, we list a summary of experimentally observed interference patterns with static magnetic phase objects. Then, we turn to pulsed magnetic fields and show that, contrary to the static case, the coherence length of the beam does not impose any limitation on the number of visible fringes. Nevertheless, it is argued that uncontrolled (though limited) experimental imperfections impinge on the interference pattern visibility. Finally, we report experimental results involving the superposition of static and time-dependent phase objects. All reported observations are consistent with the previously published theoretical description [2–5]. In Sec. IV, the results are discussed with emphasis on the prospects for realization of a longitudinal, as well as a transverse Stern-Gerlach interferometer using a succession of four magnetic-field pulses. This type of device will be very similar to the atom interferometers that use the mechanical effect of light to split the atom wave packet [6–9].

II. EXPERIMENTAL METHOD

On the one hand, the effects induced by magnetic fields on Zeeman state populations and coherences have been known for a long time and are used in many applications. On the other hand, the (historical) Stern-Gerlach experimental scheme demonstrates how magnetic-field gradients can influence the external motion of atoms [10]. It is only recently that it has been realized how the interplay between internal and external degrees of freedom might be used to build and operate atomic SGI [11,12,5].

The principle of our interferometer relies on Zeeman state preparation of a thermal beam of metastable $2s_{1/2}$ hydrogen atoms and bears similarities with optical and neutron polarization interferometers [13,14]. The experimental apparature has already been described in detail in previous publications [2–5,15]. It is schematically shown in Fig. 1. The beam of metastable hydrogen atoms $H^*(2s)$ is produced by a 100-eV electronic bombardment

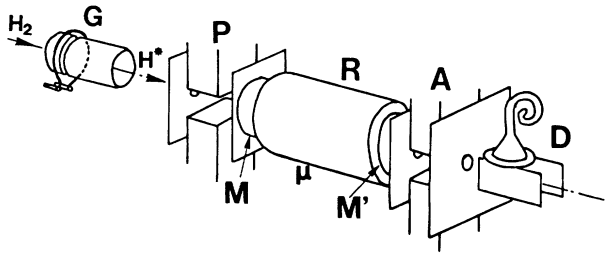

FIG. 1. Experimental setup; *G*, electron gun: *P*, *A*; polarizer and analyzer; *M*, *M'*; mixers: μ; magnetic shield: *R*; magnetic profile region (phase object): *D*; detector.

*Permanent address: St. Patrick's College, Maynooth, Ireland.

of a thermal H_2 beam within a 50-G transverse magnetic field. The beam propagating along the z axis is apertured to produce a 0.5-cm-diam beam (at the interferometer region). H^* atoms are (partially) polarized in states $2s_{1/2}$, $F=1$, $M=0,1$ by use of the Lamb-Retherford method (i.e., by use of a transverse 600-G magnetic field). Then, a coherent superposition of magnetic states is prepared within a spin twister (or "mixer") whose principle relies on a nonadiabatic evolution of the spin in a gyrating magnetic field [16]. Atoms pass through a carefully shielded magnetic phase object R. In R, the (transverse) direction of the field is kept constant ensuring an adiabatic evolution for Zeeman states $M=+1,0,-1$ referred to the y axis. Furthermore, since the field is less than 1 G no quenching via motional electric field is induced in R. Thus, each component of the prepared superposition accumulates its own phase shift ($\phi,0,-\phi$, respectively). At the output of this phase object, a new coherent superposition is built within a second spin twister and then atoms pass through an analyzer (similar to the polarizer). Downstream, the flux of emerging atoms is measured by means of a $H^*(2s)$ specific detector. It can be shown [2] that, assuming a perfect mixing, the signal is given by

$$I=\int_{v_{\min}}^{v_{\max}} dv\, f(v)\cos^4\left(\frac{\phi}{2}\right), \tag{1}$$

where $f(v)$ is the velocity distribution of the beam. The case of imperfect mixing has been discussed in previous papers and is not relevant to the present issues. The signal is recorded as a function of some scanned relevant parameter of the phase object. This yields to interference patterns whose characteristics (e.g., position of the central fringe and contrast) have been used to investigate longitudinal [17] and angular coherence [18] properties of the atomic beam. The manifestation of a topological phase of the Berry type has also been demonstrated for atoms traveling through a conical magnetic-field phase object [3].

Both metastable atom production and detection can easily be pulsed. This enables a measurement of the velocity distribution using a time-of-flight (TOF) technique as well as velocity selection. With no velocity selection, the velocity corresponding to the most probable time-of-flight t_0 is $v_1=10$ km/s. The bump in the velocity distribution for t/t_0 round 0.3 corresponds to metastable atoms produced by a different dissociation process of the H_2 molecule than that for the mean maximum [$H(2s)+H(n=2)$ instead of $H(2s)+H(1s)$]. The distance from the metastable source to the detector is approximately 38 cm. In the experiments described below, we made use of a velocity selection around v_1 and around $v_2=5$ km/s with $(\delta v/v)=12\%$. To do so, we applied for $v_1=10$ km/s, a 1-μs-wide pulse to the source electron gun followed 38 μs later by a 3-μs-wide pulse to the detector and the corresponding values for v_2. Experimental TOF spectra are given in Fig. 2 displaying the velocity distributions that have been used.

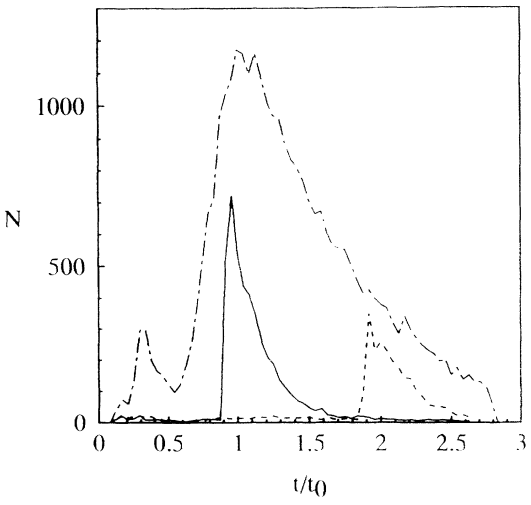

FIG. 2. Time-of-flight distribution of $H^*(2s)$ atoms. The flight path is 38 cm. The acquisition time is 3000 s, t_0 is the most probable time-of-flight. The broken line displays the full distribution. The full line corresponds to velocity selection at 10 km/s and the dotted line to 5 km/s.

III. RESULTS AND DISCUSSION

A. Interference patterns with static magnetic fields

The magnetic-field profile (phase object) is located approximately halfway between the source and the detector. It is created by an electric circuit made of five-turn wires parallel and equidistant to the beam propagation z axis transporting intensities i_H in a rectangular (100×14 mm^2) Helmholtz-coil configuration (see Fig. 3). The additional horizontal straight rectangular frame made of tow parallel wires in Fig. 3 is to be used only in Sec. III C. The Helmholtz circuit creates a magnetic field $\mathbf{B_H}(z)$ parallel to the y axis; the field is transverse but the gradient of the field is longitudinal. Moreover, because $\mathbf{B_H}$ is uniform near the middle of the phase object, the field gradient is limited to both ends of the profile. If the magnetic field is time independent, the net effect of the phase object is a longitudinal Stern-Gerlach (SG) effect. The entrance and exit gradients create longitudinal forces that act on the external motion differently for each magnetic component. This entanglement induced that both the carrier wave and the wave-packet envelope are shifted. For atoms having a velocity v, the phase shift for sublevel M is given by

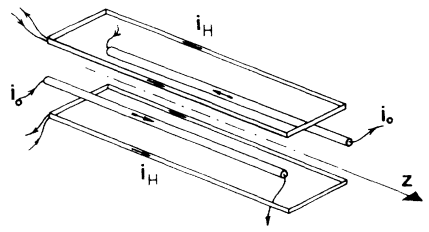

FIG. 3. Electric circuits creating the magnetic phase object in region R. Rectangular Helmholtz coils are supplied with current i_H. The rectangular frame is supplied with current i_0 in Sec. III C (i_0 is null in Secs. III A and III B).

$$\frac{\phi_{SG}}{2\pi}=\frac{2Mg\mu_B}{h\nu}\int B_H(z)dz\ , \tag{2}$$

where g is the Landé factor and μ_B is the Bohr magneton.

From this formula, the SG effect is clearly seen to be dispersive; this fact is easily demonstrated experimentally. Indeed, as displayed in Fig. 4, dividing the velocity by a factor of 2 (from v_1 to v_2) results in dividing by 2 the fringe spacing of the interference pattern validating the velocity dependence in (2). Furthermore, the contrast of the pattern gives an experimental value for the longitudinal coherence length δl of the beam. The number of visible fringes (~ 5 and ~ 9, respectively) is equal to $\delta l/\lambda$. Increasing the spectral purity of the beam by decreasing $(\delta v/v)$ for a given velocity class makes it possible to raise δl and to increase the number of visible fringes. Nevertheless, due to the dispersive character of the SG phase shift, this number is still always limited by the coherence length of the beam. To be more specific, in our experimental conditions we have $\lambda_1=38$ pm for $v_1=10$ km/s, and $\lambda_2=76$ pm for $v_2=5$ km/s with $(\delta v/v)=12\%$ for both velocity selections. The shared experimental value for the longitudinal coherence length δl is 190 pm. Furthermore, since the magnetic field (in mG) near the middle of the phase object is given by $2i_H$ (with i_H in mA), the phase shift of sublevel M is given by

$$\frac{\phi_{SG}}{2\pi}=0.56\frac{i_H(\text{mA})}{v(\text{km/s})}\ . \tag{3}$$

Thus, the experimental value 18 mA for the fringe spacing when $v=10$ km/s is in good agreement with the 17.8 mA theoretically predicted value. The same agreement holds true for a velocity equal to 5 km/s.

B. Interference patterns with pulsed magnetic fields: SAB effect

The validation of the SAB effect encompasses the utilization of both velocity selection and magnetic-field pulses. In addition to the previously described velocity selection, it is feasible to pulse the magnetic field (via the electric current i_H) with a time delay δ (between the peak of the source electron gun pulse and the beginning of the magnetic-field pulse) and a pulse duration T such that all the selected atoms are exposed to the magnetic field while being near the middle of the phase object. (It should be noticed that in the present situation and contrary to the vectorial Aharonov-Bohm effect, a semiclassical description of the external motion is needed.) Here the magnetic field experienced by the atom during the pulse duration is spatially uniform. There is, thus, no magnetic gradient force (of the Stern-Gerlach type) acting on the atom external motion. Nevertheless, each M magnetic state phase is shifted by an amount proportional to the pulse area;

$$\frac{\phi_{SAB}}{2\pi}=\frac{Mg\mu_B}{h}B_H T\ . \tag{4}$$

This effect is equivalent to the scalar Bohm-Aharonov effect for a particle of charge q submitted to a pulsed electric potential while propagating inside the interferometer arms [19–21]. To see the equivalence, one has just to formally change from the charge q to the magnetic dipole, and from the electric potential to the magnetic field. Due to practical experimental difficulties, the SAB effect has not been yet demonstrated with charged particles (e.g., in electron interferometry). On the contrary, it has been recently studied using neutron interferometry [22] in an experiment whose principle and realization are very close to ours. The relative phase shift between substates (given by the pulse area) is independent of the atom velocity. This nondispersivity is the signature of its topological nature [23]. This has the important consequence that the number of visible fringes is not related to the longitudinal coherence length δl of the beam as was the case for the Stern-Gerlach effect. These two facts are clearly demonstrated in Figs. 5 and 6. In Fig. 5, we have recorded in-

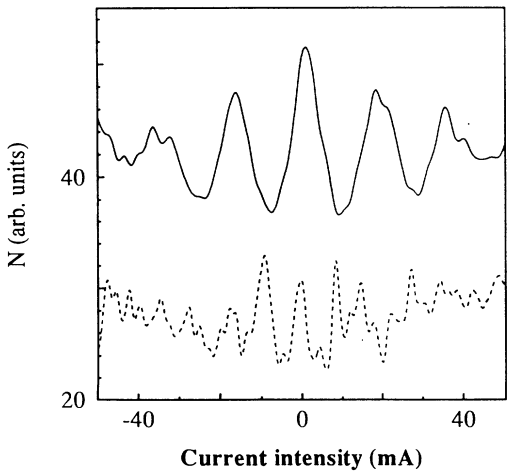

FIG. 4. SG interference patterns with velocity selection at 10 km/s (full line) and with velocity selection at 5 km/s (dotted line). $(\delta v/v)=12\%$ for both selections. The current flows in the Helmholtz coils.

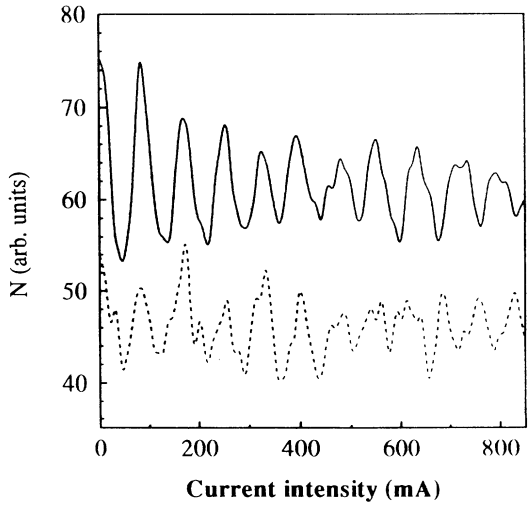

FIG. 5. SAB interference patterns with velocity selection at 10 km/s (full line) and with velocity selection at 5 km/s (dotted line). $(\delta v/v)=12\%$ for both selections. The current pulse is applied to the Helmholtz coils.

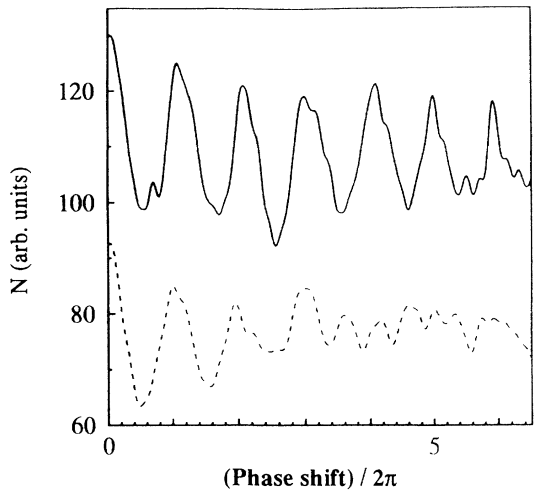

FIG. 6. SAB (full line) and SG (dotted line) interference patterns with velocity selection at 10 km/s (with $\delta v/v=12\%$).

terference patterns for the two previously used velocity classes. While the velocity ratio is two, the same spacing between fringes is obtained demonstrating the nondispersive character of the effect. The magnetic field (in mG) during the pulse is equal to $2i_H$ (in mA). Thus, for a pulse of duration T (given in μs), the phase shift is given by

$$\frac{\phi_{\mathrm{SAB}}}{2\pi}=2.810^{-3}Ti_H \ . \tag{5}$$

Thus, for the then used pulse duration ($T=3$ μs), one predicts from the preceding expression a 0.12-A fringe spacing slightly different from the 0.08-A experimental value. This discrepancy might be related to the lack of precise measurement of the real magnetic field experienced by the atoms.

In Fig. 6, we compare the interference pattern in the time-dependent (SG) situation with the one obtained in the time-dependent pulsed (SAB) situation. In both cases the same electric device (rectangular Helmholtz coils) is operated and the same velocity selection [around $v_1=10$ km/s with $(\delta v/v)=12\%$] is made. The dispersive character of the SG experiment and the nondispersive character of the SAB effect are clearly demonstrated by considering the two pattern envelopes. In the SG case, the contrast is washed out by dispersion as soon as ϕ exceeds 5π (the range of ϕ in Fig. 6 has been chosen accordingly). In the SAB case, fringes are still visible for ϕ exceeding 20π (see Fig. 5). If all the experimental conditions (for example, magnetic profile and pulse reproducibility) were perfect, there should be no limitation to the number of visible fringes in the SAB effect. In practice, there are spatial inhomogeneities and unavoidable random drifts; atoms following different "trajectories" experience slightly different phase shifts. This can be modelized by inserting in the signal expression a random phase with a Gaussian probability distribution of standard deviation σ. For an arbitrary phase shift (SG, SAB, or compound), one gets

$$I=\int_{-\infty}^{+\infty}du\frac{1}{\sqrt{2\pi}\sigma}e^{-u^2/2\sigma^2}\int_{v_{\min}}^{v_{\max}}dv\,f(v)\times\cos^4\left[\frac{\phi(1+u)}{2}\right] . \tag{6}$$

When the phase shift is velocity independent, the integration yields an analytical result

$$I=N\left(\tfrac{3}{8}+\tfrac{1}{2}\cos(\phi)e^{-(\sigma^2/2)\phi^2}+\tfrac{1}{8}\cos(2\phi)e^{-2\sigma^2\phi^2}\right) , \tag{7}$$

where N is the number of selected atoms. From expression (7), one finds that the number of visible fringes is about $1/(2\pi\sigma)$. As shown below (in Fig. 10 of Sec. III C), this tentative explanation gives fairly good agreement with the experimental data assuming σ to be 5%. In the SG (dispersive) case studied in the preceding paragraph, this effect is hidden by the more important blurring of the fringes due to the velocity spread.

Coming back to the fully deterministic SAB effect, we have investigated the effect of a fixed height pulse temporal position. This study has interesting implications for the validity of our model and for its generalization to nonhomogeneous pulsed magnetic fields. A velocity selected beam [around $v_1=10$ km/s with $(\delta v/v)=12\%$] is passed through the interferometer. The magnetic-field pulse area is chosen to give a 3π phase shift if applied while the atoms are within the uniform profile region (i.e., near the middle of region R). The proper choice of i_H is obtained from Fig. 5 for the chosen 5-μs pulse duration T. The signal is recorded as a function of the time delay δ between the source and the magnetic pulses. The results are displayed in Fig. 7. Not surprisingly, the pulse has no influence on the signal when applied when none of the atoms have entered the magnetic profile ($\delta<6$ μs) or after they have all left it ($\delta>34$ μs). The registered signal

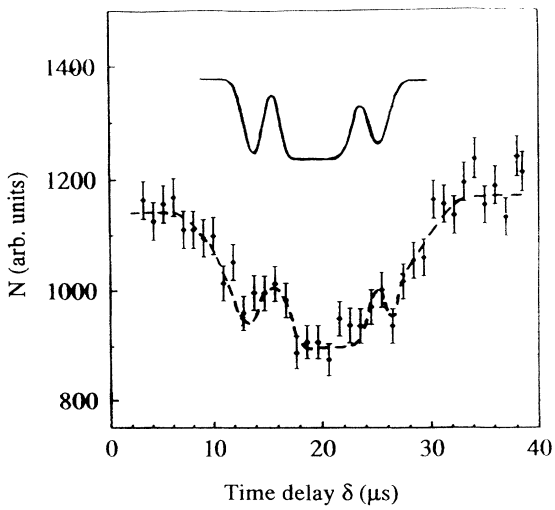

FIG. 7. Plot of the experimental signal (points) as a function of the time delay δ between source and field pulses. Pulse duration is $T=5$ μs. The velocity class $v_1=10$ km/s is selected. Pulse area is such that the full phase shift is 3π. The full line corresponds to the theoretical model. The dotted line is a guide for the eye.

corresponds then to the central bright fringe of the interference pattern. As well, the phase shift is seen to be almost constant when all the selected atoms are expected to experience the full pulse while being near the center of region R ($18\ \mu s < \delta < 23\ \mu s$). The signal then corresponds to the second dark fringe. These two results already validate some of our prerequired guesses dealing with atom "localization". However, Fig. 7 supplies supplementary information when time delays ($6\ \mu s < \delta < 18\ \mu s$ and $23\ \mu s < \delta < 34\ \mu s$) are such that for some of the selected atoms part of the pulse is experienced while the atoms are traveling through transition regions at both verges of R in which the magnetic field is spatially inhomogeneous. Then the distinction between SAB and SG effects has to be carefully reanalyzed. Nevertheless, since our time resolution is not properly adapted to that required, we can limit ourselves to a crude model (spin precession) in which the variable part of the signal is given by

$$\cos^4\left[\frac{Mg\mu_B}{\hbar}\int_{t_p}^{t_p+T} dt' B_H(v_1 t')\right], \tag{8}$$

where t_p is the beginning time of the magnetic-field pulse. To fit the experimental data, one has to average (8) in order to take into account the t_p and the velocity dispersions related to the time extension of the gun pulse and of the velocity selection procedure. Figure 7 shows a good agreement between the calculation based on this model and the experimental data. To go beyond this first attempt to look at the effect of pulsed forces requires a more refined experimental procedure. The longitudinal magnetic-field gradient would have to be properly controlled and of greater spatial extension to avoid the need for very short pulse duration and prohibitive velocity selection. Works are currently in progress and results will be reported in a forthcoming study.

C. Experimental tests for phase-shift additivity

SAB and SG effects appear in two very different ways when the atom wave packet is treated as a carrier wave modulated by a slowly varying envelope [4,20]. In SAB, the carrier wave is shifted while the envelope remains unperturbed. This feature explains why the contrast remains constant even for high interference orders. On the contrary, in the static SG case, both the carrier and the envelope experience a shift. From this standpoint, the result of the combination of SAB and SG effects is not easy to handle. In this section, we address this question. To do so, we examine the effect of the addition of a static magnetic phase object to the pulsed magnetic field studied in Sec. III B. To provide a static magnetic field (i.e., the SG phase shift ϕ_{SG}), use is being made of the frame made of two five-turn electric wire arrangement transporting intensity i_0 (see Fig. 3) while the Helmholtz coils are used to provide the pulsed field (i.e., the SAB phase shift ϕ_{SAB}). In the two sets of experiments described below, we use the following experimental conditions: velocity selection around $v_1 = 10$ km/s with $\delta v/v = 12\%$; pulse delay is 18 μs and duration T is 5 μs. Thus, all the selected atoms experience the full pulse while being near the middle of the phase object (SAB conditions).

In the first set of experiments, SAB interference patterns are registered (see Fig. 8) as previously done in Sec. III B but now with the addition of a static permanent current i_0, whose amplitude is chosen such as the corresponding phase shift ϕ_{SG} is π or 5π. One gets interference patterns very similar to those of Fig. 5. The SAB interference pattern without any static field is displayed for comparison. One obtains for all the cases, visible fringes for ϕ_{SAB} as high as 14π. The contrast is thus seen not to be limited by the coherence length δl of the beam. Furthermore, the whole SAB fringe patterns are shifted by the SG effect since for $\phi_{SG} = \pi$ or 5π one gets dark fringes in place of bright ones (for $\phi_{SG} = 0$) and vice versa. The atom phase shift additivity $\phi = \phi_{SG} + \phi_{SAB}$ is thus validated.

In a second set of experiment, fixed and scanned parameters are interchanged; SG interference patterns are registered (see Fig. 9) as a function i_0 (i.e., of ϕ_{SG}) as in Sec. III A but, now, with addition of a magnetic-field pulse whose area is chosen such that the corresponding phase shift ϕ_{SAB} is π or 5π. One gets interference patterns very similar to those of Fig. 4. The interference pattern without any field pulse is displayed for comparison. The envelope width of the three given interference patterns is seen to be related to the coherence length δl of the beam as was discussed in Sec. III A. Only five fringes are visible. The SG fringes are shifted by the SAB effect since for $\phi_{SAB} = \pi$ or 5π one gets a dark fringe for null i_0. The phase additivity $\phi = \phi_{SG} + \phi_{SAB}$ is thus again validated.

A somewhat surprising result is found if one considers carefully the envelopes in the cases where both SG and SAB effects are present. Indeed, the maximum contrast is not obtained for null values of the scanned parameter. We interpret this shift of the interference pattern envelope as being due to the experimental imperfections al-

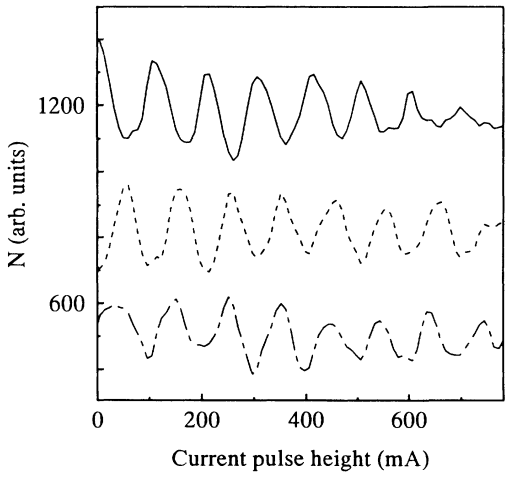

FIG. 8. (SAB) interference patterns in presence of a static magnetic such that $\phi_{SG} = \pi$ (middle dashed line) or $\phi_{SG} = 5\pi$ (bottom dashed line). Full line is the SAB pattern without additional static field.

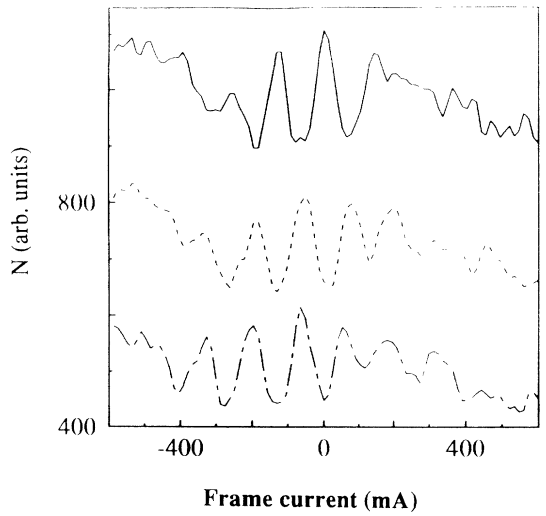

FIG. 9. (SG) interference patterns in presence of a SAB phase shift due to the addition of a magnetic-field pulse of given area: $\phi_{SAB}=\pi$ (middle dashed line) and $\phi_{SAB}=5\pi$ (bottom dashed line). Full line is the SG pattern without additional field pulse.

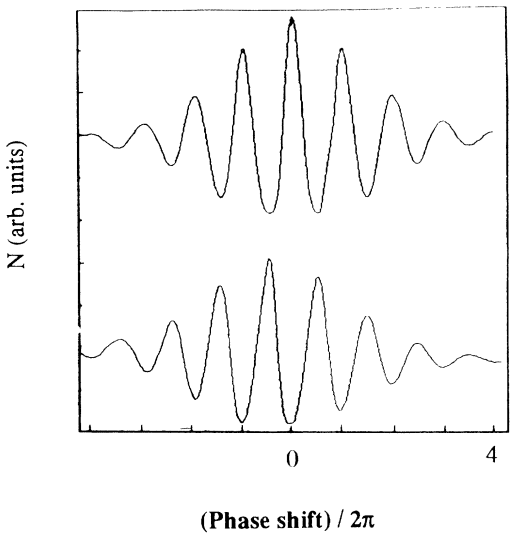

FIG. 11. Numerical simulation deriving from Eq. (6) with $\sigma=5\%$. ϕ_{SG} is scanned for $\phi_{SAB}=0$ (upper curve) and $\phi_{SAB}=5\pi$ (lower curve).

ready discussed in Sec. III B to explain the limitations of the SAB fringe visibility. Using the same model as in Sec. III B (addition of a random phase), the theoretically predicted signal is given by Eq. (6) where $\phi=\phi_{SG}+\phi_{SAB}$ is the atom total phase shift. Figure 10 gives the numerical results derived from (6) with $\sigma=5\%$ when ϕ_{SAB} is scanned for zero and 5π values of ϕ_{SG} (these values being determined for the mean velocity of the selected class). To enhance the effect of the random phase in the numerical simulations, the value of the standard deviation σ of the Gaussian distribution has been slightly increased compared to the more realistic 3% value derived in the preceding paragraph. Nevertheless, a fairly good agreement with the experimental results of Fig. 8 is met, including the envelope slight shift. Figure 11 gives the same type of numerical results (with $\sigma=5\%$) when ϕ_{SG} is scanned for zero and 5π values of ϕ_{SAB}. Once again, agreement with the experimental results (Fig. 9) is met, including the envelope shift. It should be noticed here that the dispersivity of the SG effect enables an analytical calculation of the signal. The relevance of experimental imperfections must be stressed since now their effect (shift of the pattern visibility) is most important. Apart from this subtle experimental effect, we can conclude that SG and SAB phase shifts can be added to get the total atom phase shift when both static fields and pulsed homogeneous fields are present.

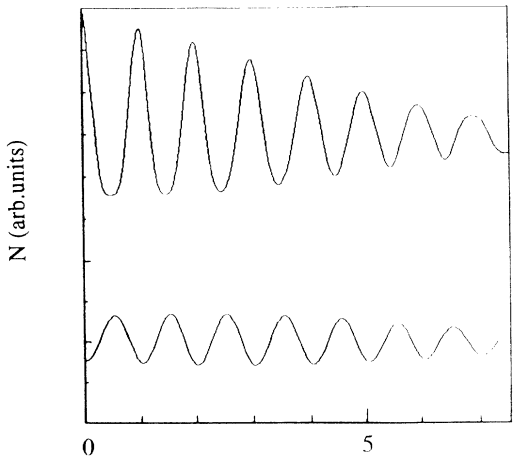

FIG. 10. Numerical simulation deriving from Eq. (6) with $\sigma=5\%$. ϕ_{SAB} is scanned for $\phi_{SG}=0$ (upper curve) and $\phi_{SG}=5\pi$ (lower curve).

IV. SUMMARY AND CONCLUSIONS

The principles of experimental Stern-Gerlach interferometry have been reviewed. The nondispersive character of the scalar Bohm-Aharonov effect has been clearly demonstrated. The dispersive character of the corresponding static magnetic-field configurations has been shown as opposed to the former. The question of phase additivity has been addressed by combining a static magnetic field and a pulsed magnetic field. It has been shown that experimental imperfections have to be taken into account to get the agreement between experimental observations and the theoretical description of Stern-Gerlach interferometry. Extending the present time-dependent magnetic-field studies to a spatially inhomogeneous profile is a worthwhile challenge. Indeed, important theoretical issues are to be met in this case. Since one is faced with inelastic effects via the pulsed magnetic force, the predicted signal gives information concerning off-diagonal elements of the matrix density in momentum representation. This situation is in contradiction with the static longitudinal SG effect where only diagonal matrix elements are concerned. From the practical standpoint, a thorough comprehension of the effect of pulses on atomic

coherences is valuable if one aims to realize an interferometer with four successive pulses. Such an interferometer would be the longitudinal version of the transverse interferometer proposed by Wigner [11] (see also [12]).

Experiments to be reported demonstrate that a nondispersive behavior for the atomic phase shift is also obtained with pulsed magnetic fields whose profiles exhibit an homogeneous transverse gradient (anti-Helmholtz configuration) [24]. Since the wave packet is then splitted transversally, these results open the way to the realization of a Stern-Gerlach interferometer with separated arms. Such a device involving four pulses in a proper geometry, will parallel the interferometers using four interaction zones with laser beams in the Ramsey configuration [6–8] or those using light pulses acting on stimulated Raman transitions [9] with the use of a permanent magnetic dipole in place of optical dipoles. This suggests new avenues for practical applications of Stern-Gerlach interferometry.

ACKNOWLEDGMENTS

The authors would like to thank Dr. M. Devoret and Professor K. Rubin and Professor B. Englert for valuable suggestions. This work has been supported by EC Contract No. SC1*-CT91-0712 (TSTS). One of us (S.N.C.) thanks the EC Commission for the provision of a Science Bursary Contract (No. B/SCI*915186), Laboratorie de Physique des Lasers is Unité Associée du CNRS, URA 282.

[1] For a recent review, see *Optics and Interferometry with Atoms,* edited by J. Mlynek, V. Balykin, and P Meystre, special issue of Appl. Phys. B **54**, 319 (1992).
[2] J. Robert, Ch. Miniatura, O. Gorceix, S. Le Boiteux, V. Lorent, J. Reinhardt, and J. Baudon, J. Phys. II **2**, 601 (1992).
[3] Ch. Miniatura, J. Robert, O. Gorceix, V. Lorent, S. Le Boiteux, J. Reinhardt, and J. Baudon, Phys. Rev. Lett. **69**, 261 (1992).
[4] S. Nic Chormaic, Ch. Miniatura, O. Gorceix, B. Viaris de Lesegno, J. Robert, S. Feron, V. Lorent, J. Reinhardt, J. Baudon, and K. Rubin, Phys. Rev. Lett. **72**, 1 (1994).
[5] J. Robert, Ch. Miniatura, S. Le Boiteux, J. Reinhardt, V. Bocvarski, and J. Baudon, Europhys. Lett. **16**, 29 (1991).
[6] Ch. Bordé, Phys. Lett. A **140**, 10 (1989).
[7] F. Riehle, Th. Kisters, A. Witte, J. Helmke, and Ch. Bordé, Phys. Rev. Lett. **67**, 177 (1991).
[8] U. Sterr, K. Sengstock, J. H. Müller, D. Bettermann, and W. Ertmer, Appl. Phys. B **54**, 341 (1992).
[9] M. Kasevich and S. Chu, Phys. Rev. Lett. **67**, 181 (1991).
[10] W. Gerlach and O. Stern, Z. Phys. **8**, 110 (1922).
[11] E. P. Wigner, Am. J. Phys. **31**, 6 (1963).
[12] B.-G. Englert, J. Schwinger, and M. O. Scully, Found. Phys. **18**, 1045 (1988); Z. Phys. D **10**, 135 (1988); Phys. Rev. A **40**, 1775 (1989).
[13] M. Born and E. Wolf, *Principles of Optics,* 6th ed. (Pergamon, Oxford, 1980).
[14] F. Mezei, Physica **137B**, 295 (1986), and Refs. therein.
[15] Ch. Miniatura, F. Perales, G. Vassilev, J. Reinhardt, J. Robert, and J. Baudon, J. Phys. II **1**, 425 (1991).
[16] Ch. Miniatura, J. Robert, S. Le Boiteux, J. Reinhardt, and J. Baudon, Appl. Phys. B **54**, 347 (1992).
[17] S. Nic Chormaic, V. Wiedemann, Ch. Miniatura, J. Robert, S. Le Boiteux, V. Lorent, O. Gorceix, S. Feron, J. Reinhardt, and J. Baudon, J. Phys. B **26**, 1271 (1993).
[18] J. Robert, Ch. Miniatura, S. Nic Chormaic, O. Gorceix, F. Perales, and J. Baudon, J. Phys. (France) II **4**, 1 (1994).
[19] Y. Aharonov and D. Bohm, Phys. Rev. **115**, 485 (1959).
[20] A. Zeilinger, J. Phys. (Paris) Colloq. **45**, C3-213 (1984); in *Fundamental Aspects of Quantum Theory,* Vol. 144 of NATO Advanced Study Institute, Series B: Physics, edited by V. Gorini and A. Frigerio (Plenum, New York, 1985), p. 311.
[21] J. Anandan, in Proceedings of the third International Symposium on Foundations of Quantum Mechanics, edited by Editors (Physical Society of Japan, Tokyo, 1989), p. 98.
[22] G. Badurek, H. Weinfruter, R. Gähler, A. Kollmar, S. Wehinger, and A. Zeilinger, Phys. Rev. Lett. **71**, 307 (1993), and Refs. therein.
[23] W. H. Furry and N. F. Ramsey, Phys. Rev. **118**, 623 (1960).
[24] J. Robert, O. Gorceix, J. Lawson-Daku, S. Nic Chormaic, Ch. Miniatura, J. Baudon, F. Perales, M. Eminyan, and K. Rubin, in Fundamental Problems in Quantum Theory, edited by D. Greenberger, Proceedings of the New York Academy of Sciences, The Annals of the New York Academy of Sciences (in press).